REVIEW

Check for updates

Biomimicking spider webs for effective fog water harvesting with electrospun polymer fibers

Joanna Knapczyk-Korczak [ID] and Urszula Stachewicz [ID] *

Fog is an underestimated source of water, especially in regions where conventional methods of water harvesting are impossible, ineffective, or challenging for low-cost water resources. Interestingly, many novel methods and developments for effective water harvesting are inspired by nature. Therefore, in this review, we focused on one of the most researched and developing forms of electrospun polymer fibers, which successfully imitate many fascinating natural materials for instance spider webs. We showed how fiber morphology and wetting properties can increase the fog collection rate, and also observed the influence of fog water collection parameters on testing their efficiency. This review summarizes the current state of the art on water collection by fibrous meshes and offers suggestions for the testing of new designs under laboratory conditions by classifying the parameters already reported in experimental set-ups. This is extremely important, as fog collection under laboratory conditions is the first step toward creating a new water harvesting technology. This review summarizes all the approaches taken so far to develop the most effective water collection systems based on electrospun polymer fibers.

1. Introduction

For thousands of years, access to drinking water has been the key to survival. This is the reason why water has become a symbol of life. Water supplies are one of the global challenges[1] due to climate changes[2] and the quality of water which may be harmful to human health.[3] In spite of technological developments, people are still seeking new water collection strategies, and many ideas are inspired by nature.[4–8] A number of solutions are based on animal and plant strategies for collecting water from humid air, *e.g.* Namib Desert beetles (*Stenocara gracilipes* and *Onymacris unguicularis*), Australian thorny devil

AGH University of Science and Technology, Faculty of Metals Engineering and Industrial Computer Science, al. A. Mickiewicza 30, 30-059 Kraków, Poland. E-mail: ustachew@agh.edu.pl

Joanna Knapczyk-Korczak is a young researcher at the AGH University of Science and Technology in Krakow (Poland). She earned her BSc and MSc degrees in materials science from the Faculty of Non-Ferrous Metals and Faculty of Materials Science and Ceramics. Currently, she is a PhD candidate in the Faculty of Metals Engineering and Industrial Computer Science. In her research, she investigates the wetting and mechanical properties of electrospun polymer fibers for fog water collection. Her research interest extends to electrospinning technology and wetting phenomena on polymer surfaces.

Joanna Knapczyk-Korczak

Urszula Stachewicz is currently an associate professor at the AGH University of Science and Technology in Krakow, Poland, where she obtained her Habilitation (DSc) in 2017. She graduated from the Delft University of Technology with a PhD in electrohydrodynamic processes and conducted her postdoctoral study at the Queen Mary University of London while working at spin-out company Nanoforce Technology Ltd, UK. Her research is focused on electrospun polymer fibers for tissue engineering and for energy and water harvesting. Her interest is in correlative and advanced microscopy and in situ mechanical testing of synthetic and naturally structured materials.

Urszula Stachewicz

lizards (*Moloch horridus*),[9,10] cactuses (*Opuntia microdasys*, *Copiapoa cinerea*, *Mammillaria columbiana*, *Parodia mammulosa*),[11,12] desert grass (*Stipagrostis sabulicola*, *Setaria viridis*),[6,7,13] and ferns (*Nephrolepis auriculata*).[14] Certain vascular plants use their sunlight-driven systems to produce clean water.[15] In addition to numerous plants, spider threads and silk are fascinating materials:[16,17] strong and extremely tough,[18–20] wet-adhesive,[21] but, most importantly, able to collect water by combining hydrophobic and hydrophilic properties.[22] The developing fog collection technologies show great potential in water harvesting, which can certainly contribute to and improve our living standards.[23–27] People started imitating nature by creating fog water collectors (FWCs).[28,29] FWCs are enormous nets spread out on steel stands[30,31] to collect water from the humid air, *e.g.* fog or dew, and provide it to regions where access to water resources is difficult or greatly limited.[32] The efficiency of FWCs may be high, but it is dependent on environmental conditions such as wind, fog flow, and the amount of water dispersed in the fog.[33,34] The efficiency of standard FWCs with an area of 48 m^2 can reach 3–10 L m^{-2} day^{-1}.[29,32,35] The shade coefficient of standard Raschel meshes is low and arrives at 35%[29,31] (Fig. 1). In FWCs a double layer of Raschel mesh is mounted where the area open to the passing wind is from 40%.[29] Existing FWCs are still being modified to eliminate the pore blockage by collected droplets, and the re-entrainment of the water collected from ribbons by the wind.[36–38]

Nano- and microfibers produced *via* electrospinning are characterized by a high surface area,[39] toughness,[40–42] and mechanical strength.[43,44] These qualities are beneficial not only for water collection but also in other applications such as tissue engineering, skin treatment, air filtration, water purification, smart textiles, and optoelectronic devices.[45–53] Electrospinning makes it possible to produce polymer fibers from artificially obtained silk with high mechanical properties.[54–56] The electrospun silk includes non-crystalline fibroin caused by rapid fiber formation and shows a lateral

modulus reaching 8.0 GPa.[55] Electrospun fibers have generally been investigated in terms of their super-hydrophobicity[57] and oleophobicity,[58] which are related to their surface roughness,[59–61] fiber morphology,[62] and surface modifications.[63]

The production of fibers by electrospinning is relatively cheap and efficient.[64] Electrospun fibers used in filtration are mass-produced for at least three decades. A relatively high cost is only the purchase of electrospinning pilot equipment based on a multi-nozzle system or free surface electrospinning, also called nozzleless.[46,65] Additionally, the cost of mass production depends on the type and price of selected polymers and used solvents. Therefore, the cost of producing fiber mesh for fog collection is reasonable as mainly the commonly used polymers are selected.

Water harvesting continues to be a global challenge. Therefore, in this review, we showed how nano- and microfibers can enhance the fog water collector technologies currently used. We compared the efficiency of fog water collection by new fiber structures to show the importance of their application. This review also includes the guidelines for testing new design meshes under laboratory conditions and points out the differences in the currently used experimental settings. We also discussed the important issue of droplet collection and drainage systems from meshes by using hydrophobic and hydrophilic fibers and their combinations, such as Janus systems. Importantly, the strategies for designing biomimetic meshes inspired by spider webs[66] and many plants[67] with a view to increasing the water collection efficiency were described, thus paving the way for the future development of new fog collector systems.

2. Spider webs

Spider silk is an amazing material that spiders use for many applications, such as building their cocoon, making a spider web, and wrapping their prey.[68] Silk fibers can withstand the
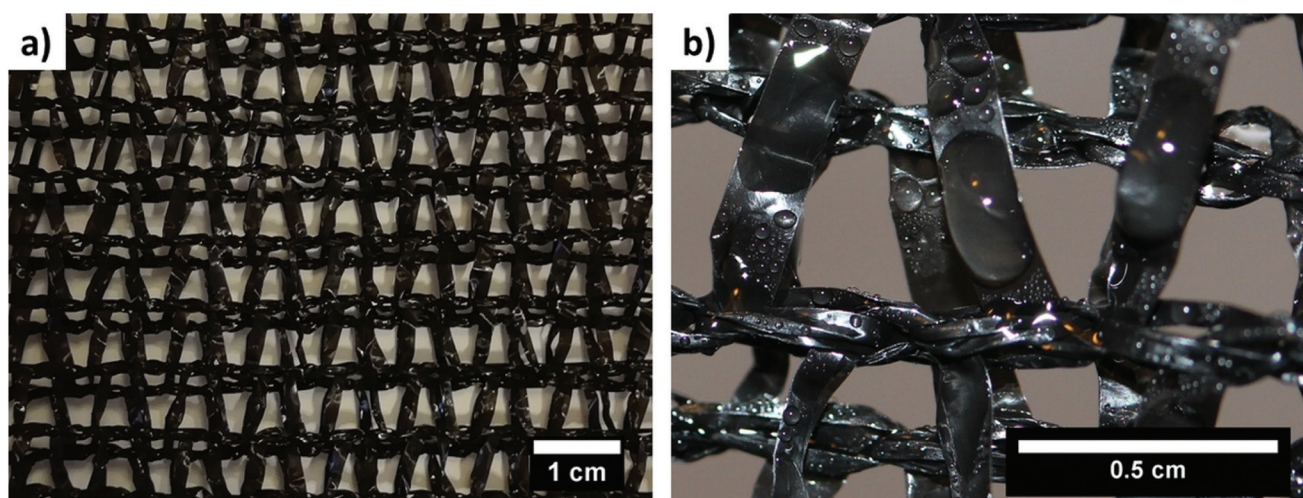

Fig. 1   Images of (a) a typical double layer of a Raschel mesh and (b) water droplets collected on a Raschel mesh.
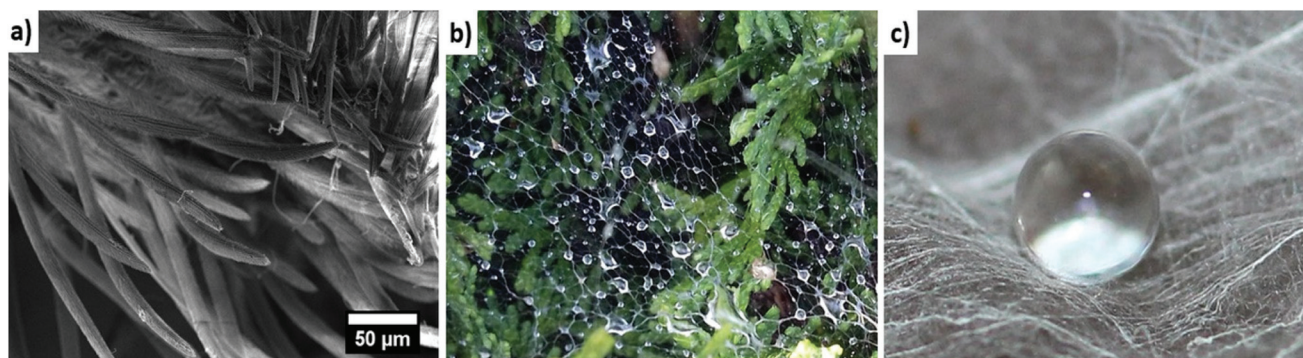
Fig. 2 (a) Scanning electron microscopy (SEM) micrograph of spider spinnerets of *Grammostola pulchra*; (b) photograph of water droplets captured on a spider web in nature; (c) the water droplet deposited on a *Linothele Megatheloides* web that was wrapped around a piece of wood, evidencing the superhydrophobic property of this web.

spider's weight and absorb the energy of the insect trapped in the web.[69,70] Spiders produce threads *via* special spinnerets on their abdomen[71,72] (Fig. 2a). The thread obtained is the product of a secretion from the spider's body.[73,74] Initially, the secretion is a high-viscosity fluid that becomes a solid thread as it passes through papillary glands. The secretion is produced by many glands, depending on the spider's sex.[16,75] Males develop five glands, while females have up to seven; the difference is related to the females' role of having and caring for offspring. Spiders produce silk with different properties for many purposes;[76–78] in particular, their thread strength varies among the different spider species. The strongest fibers are produced by *Caerostris Darwini*, reaching 1652 MPa while, by comparison, *Gramostola Rosea* makes one of the weakest fibers, with a strength of 20 MPa.[69]

Spider silk consists of different proteins, often called *spidroins*, created by combining the words spider and fibroin, which are the structural core of the silk. This name distinguishes spider fibroins from fibroins produced by silkworms.[79,80] A number of environmental factors affect the extraordinary mechanical properties of silk.[18,68] The chemical composition of spidroins, which consist of variable repeating amino acid motifs, strongly depends on spider species.[20,81,82] The majority of ampullate spidroins (MaSp), which are structural spidroins, make the dragline silk comprising MaSp1 and MaSp2.[83] The core region of spider silk is covered by various biomolecules like glycoproteins or lipids. The wetted silk often shows different mechanical properties due to the presence of proline. However, to enhance the silk properties, it is more important to have a pair of hydrophobic–hydrophilic spidroins. Importantly, different spider species have shown that the MaSp1/ADF4 combination exhibits more hydrophobic character than MaSp2/ADF3.[83,84] Additionally, some spiders catch preys by covering the web with sticky glue or by using the electric charge generated on the web.[85–87] The sticky glue is comprised of glycoproteins, a combination of hygroscopic low molecular mass organic and inorganic compounds (LMMCs) and water.[78,85] This coating enables the fibers to adhere to one another. Silk is spun not only by spiders but also many arthro-

pods, like arachnids, insects and myriapods, which are able to produce this biopolymer.[88] Interestingly, silk produced by silkworms, *e.g.*, by a Bombyx mori species, is significantly different from spider silk. It consists of two main proteins: silkworm fibroin and sericin. The content of sericin ranges from 25 to 30% of silk proteins. It helps the cocoon formation by forming the sticky layer around the fibroin fibers. Sericin is hydrophilic as it contains a large number of amino acids with neutral polar functional groups.[89,90] Spider and silkworm silk differ not only by the structure of the organization of the nanofibril clusters. The silkworm cocoon thread can be three times bigger than the spider dragline.[88]

The spider web is an excellent example from nature of how fibers can collect water from the environment.[6,66,91] They can collect water droplets from drizzle, fog, or condensation processes (Fig. 2b). The spider web is hydrophobic, and water droplets collected on the web create a round shape[92] (Fig. 2c). The droplet observed in this image lies on a cobweb produced by *Linothele Megatheloides.* This is a fast arboreal spider that belongs to the Dipluridae family, which lives in the tropical forests of Colombia.[93–95] It grows up to 11 cm in length including its legs, and is characterized by a slim silhouette. Interestingly, this spider has the largest spinneret in the world, which enables it to spin an enormous amount of silk.

The production of bionic spider silk is also possible thanks to transgenic goats and silkworms, which were genetically modified to produce spider spidroin.[96–99] The spidroin is secreted to goat milk, where they are later recovered and electrospun. The genetic modification of silkworms made them possible to spin spider spidroins instead of normal silkworm silk, which consists of fibroin and sericin.

3. Micro- and nanofibers

New material technologies revolutionize the world, especially at the micro- and nanoscale levels, thanks to the many new application possibilities.[39,100–105] Micro- and nanofiber polymers boast state-of-the-art properties compared to raw

materials[106,107] and are often produced using one of the most versatile methods, such as electrospinning.[47,51,108] This process makes it possible to obtain fibers from melt polymers[109] or polymer solutions using an electric field.[110] The voltage is usually applied to a metal nozzle, from which the material flows, forming a cone-jet. In electric fields, the polymer jet starts to spin, producing fibers that are deposited on the counter electrode, ground, or connected to the opposite voltage[111–113] (Fig. 3a). The advantage of electrospinning is that various nozzles can be used, such as co-axial[114] or side-by-side,[115] as shown in Fig. 3b and c. The different designs of nozzles and needles[116–118] include the standard single nozzle, which is commonly used to obtain fibers from uniform polymer solutions[119,120] or several solution blends.[121,122] Standard nozzles are often multiplied to increase the efficiency of fiber production.[123]

Electrospun fibers can be produced from many, often incompatible, solvents to obtain complex fibrous composites,[124] including electrospinning a few polymers at the same time or in a layer-by-layer process.[48,49,125] However, the compatibility of solvents used in co-axial or side-by-side electrospinning is crucial to avoid the early solidification of polymers.[126,127]

The essence of electrospinning is relatively simple, but the formation of fibers with specified morphology and desirable properties requires extensive knowledge and research experience due to the many parameters affecting the stability of the process.[128–130] Fiber morphologies can be manipulated thanks to many parameters involved in preparing the solution and the process itself. The polymer concentration in the solution and an appropriate selection of solvents make it possible to obtain fibers that are either smooth and beadless or beaded[131] (Fig. 4a and b). Usually, beads form in fibers when the polymer concentration in the solution is too low.[132] The fiber diameter is affected not only by the polymer concentration and molecular mass, but also by solvent volatility.[127,133–136] Three main parameters control the stability of electrospinning: polymer flow rate, the distance between the nozzle and collector, and the voltage applied.[137–139] It is essential to have an electrospinning setup equipped with an environmental chamber with controlled temperature (T) and relative humidity (RH) if reproducible results are to be obtained. A controlled environment during the manufacture of polymer fibers makes it possible to escalate the porosity or wrinkling of fibers by increasing the RH level in the chamber.[140–148] The high RH slows down the evaporation of the solvent, which often leads to a porous structure with regular pore size and arrangements.[149] One of the advantages of porous structures is their high water absorption capacity, making them suitable for water storage applications.

The voltage polarity applied to the nozzle is the other parameter controlling the surface and mechanical properties of electrospun fibers.[45,150–152] Using a positive or negative voltage polarity causes the reorientation of the polymer chains, which can tailor the surface electric charge of individual fibers.[153–156] In addition, an external UV treatment for obtaining the *in situ* cross-linking of the polymers,[157] magnetic field assistance for controlling fiber alignment,[158] and ultrasound for generating solution protrusion[159] can be incorporated into the electrospinning setup.

The range of electrospun polymers – including hydrophobic and hydrophilic ones – is constantly growing.[61,160] The wetting
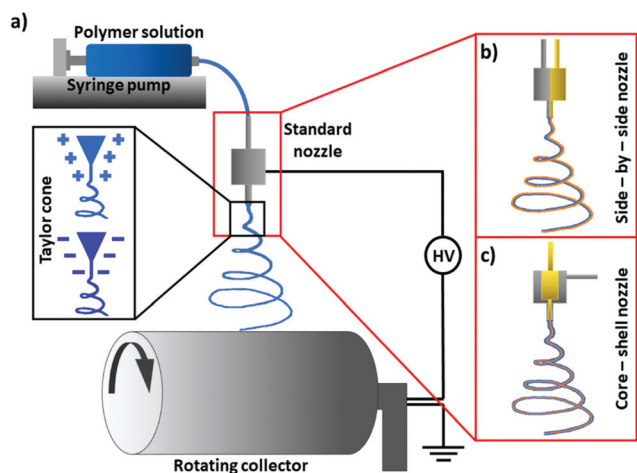
Fig. 3 Scheme of electrospinning with (a) a standard nozzle; (b) a side-by-side nozzle; (c) a co-axial nozzle, showing the principle of the electrospinning process: high voltage is applied to the nozzle and deposition takes place on the collector, which is presented here as a rotating drum.
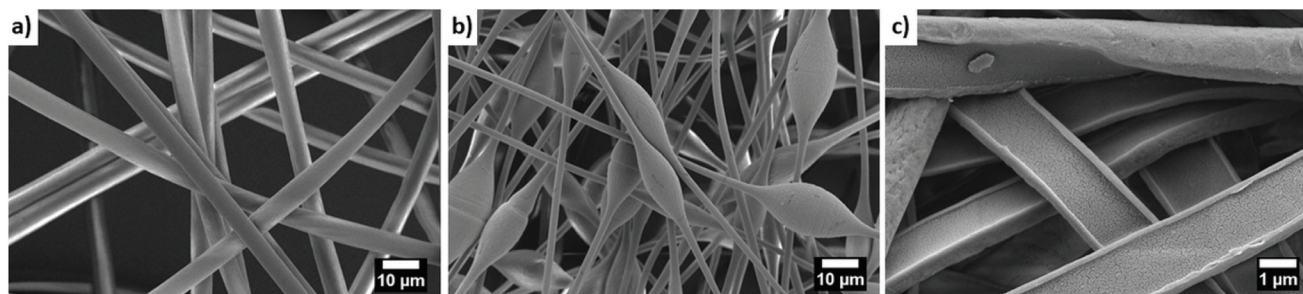
Fig. 4 SEM micrographs showing electrospun PS fibers: (a) smooth and uniform; (b) with beads; (c) gutter shape PS-CA fibers produced with a side-by-side nozzle.

properties of electrospun polymer fibers mainly depend on surface chemistry, mesh geometry, and fiber morphology.[59,161–165] The combination and manufacture of hydrophobic–hydrophilic structures are gaining popularity,[166–168] imitating a strategy often used by the nature.[7,169–171] Janus structures are commonly used in materials science, where the composite has different parts characterized by hydrophobic and hydrophilic properties.[172–174] A combination of fibers with different wetting properties in the mesh can also be designed as a layered or sandwich-type system.[175] Notably, hydrophobic–hydrophilic composites can be produced directly *via* electrospinning using side-by-side, co-axial, or multi-nozzles.[176,177] The electrospun meshes with different wetting properties and mechanical properties[178,179] can strengthen composite meshes[124,180] and increase the water collection from fog.[181–183] An image of side-by-side fibers from hydrophobic–hydrophilic materials is shown in Fig. 4c.

The effective water collection from surfaces depends on the material's ability to remove water, roll off droplets, from them. Fast water removal is necessary to reduce the blockage of pores in meshes.[36] These materials are often characterized by lower contact angle hysteresis, which makes it easier to transport smaller droplets from the mesh to the container.[184] Importantly, to decrease water contact angle hysteresis, the combination of hydrophilic and hydrophobic properties is necessary.[185,186] The hydrophilic part attracts more water from fog, but it retains them on its surface much longer than the hydrophobic part. The solution is the hydrophobic–hydrophilic combination for designing effective meshes for water collection, where the hydrophobic part has higher capabilities in removing water. Electrospun fibers are often applied in the biomimicking system of spider's web due to their dimensions and mechanical properties.[16,88,187] Another advantage of using nanofibers for water collection is the increased area used to effectively collect water droplets.

Electrospinning makes it possible to mimic nature and create structures similar to spider webs.[92] Natural fibers can be successfully imitated by fibers obtained *via* electrospinning, as electrospun fibers have a geometry similar to that of spider threads (Fig. 5). The analysis of *Linothele Megatheloides* threads shows that the bundles of silk fibers and electrospun individual polyvinylidene fluoride (PVDF) fibers have an identical wrinkled surface. The 3D shape of spider bundles and PVDF fibers was confirmed by their cross-sectional analysis using a focused ion beam – scanning electron microscope (FIB-SEM),
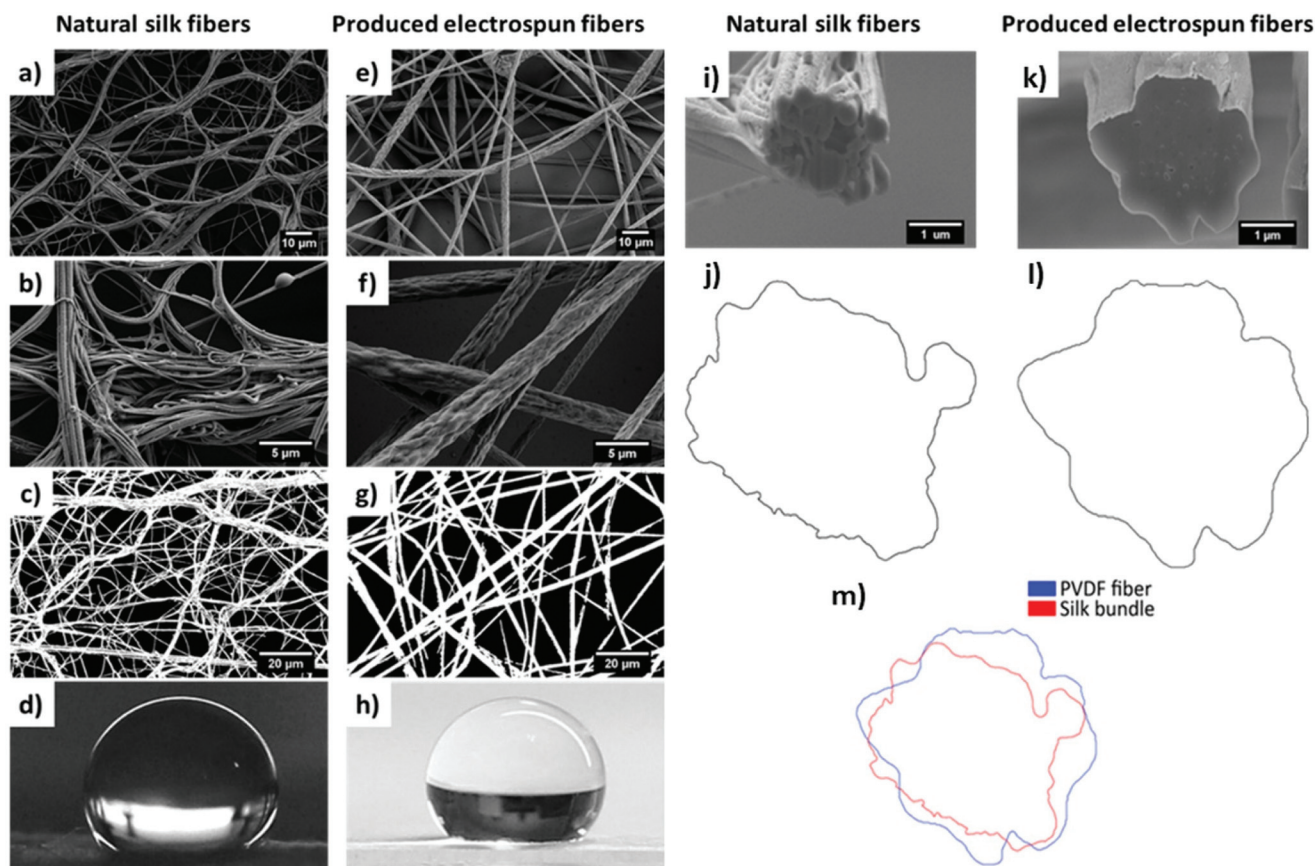

Fig. 5 SEM micrographs of (a), (b), and (i) silk fibers and bundles from a *Linothele Megatheloides* web and (e), (f), and (k) electrospun PVDF fibers; (c) and (g) processed images for the calculation of the fraction of fibers; (d), (h) images of the droplet of water used to measure contact angles; (j), (l), (m) contour images of a spider thread and PVDF fiber. Adapted and reproduced with permission.[92]

(Fig. 5m). The wetting properties of both kinds of fiber meshes showed hydrophobic features with a contact angle of 128° on PVDF and 130° on a *Linothele Megatheloides* spider web.[92]

4. Water collection challenges and key features for the meshes

Droplet sizes

Water collection from fog is more challenging than water harvesting from rain because the droplet size is smaller, ranging from 15 to 20 μm,[188] but it can arrive at up to 50 μm,[189] making it harder to collect than rainwater. Meshes with a small fiber diameter have a wider surface area, thus catching tiny fog droplets. In terms of laboratory research studies, it is challenging to simulate the natural fog because the droplets produced from ultrasonic humidifiers range from 200 to 1250 nm, while those from nano mist humidifiers measure less than 100 nm.[190] Natural fog has a much larger average droplet size because water particles have more time to coalesce together. Droplets suspended in the fog are caught by the fibers in meshes as they pass through. The captured droplets merge into larger sizes to run down by gravity. Surface roughness has great importance in wetting and shaping the water contact angle.

Roughness of meshes

Spiders can optimize fibers and webs used for harvesting water in order to maximize their water-collection capacity. Similarly, spindle-bead microfibers with cavity beads were fabricated to mimic the high efficiency of natural fibers in water collection. The designs with the desired surface roughness and mechanical strength show a long life and improved water collection efficiency *via* controlled directional water transportation.[191–194] Importantly, the droplet size, *i.e.* its volume, has a critical effect on wetting and water spreading on fibers.[195] The transport of liquid droplets can also be controlled *via* structured surfaces in many applications.[196] In terms of surface roughness, the fog deposition and water drainage system can be enhanced in the same way as on a Gunnera leaf,[197] which is roughly textured with asymmetric fibers.[198,199] Designing rough surfaces of fibers with controlled surface chemistry promotes the directional water transport from them in bridging fog droplet deposition and importantly improves the water drainage system.[198]

The wetting properties of polymer fibers also depend on many factors such as geometry,[165] roughness and surface chemistry,[59,60] voltage polarity, and surface potential.[156] In many cases, however, when we use electrospun polymer fibers, the advancing contact angle (θ) can change because of surface profilometry. Differences in material roughness can change the wetting properties of this material without affecting its surface chemistry.[59,61,200] The best examples of this are hydrophobic fibers (127 ± 3°) and hydrophilic smooth films (55 ± 3°) from cellulose acetate.[126] In that case, the water contact angle

only depended on mesh geometry because the polymer molecular weight was the same for fibers and films.[201,202]

Wetting of individual fibers

The spider web is covered with a special glue that creates characteristic beads on individual threads.[203] This sticky glue endows silk fibers with unique properties and enables them to catch insects and collect water more effectively. Fundamental studies of wetting on single fibers have shown a significant influence of the fiber morphology on droplet behavior.[204] Research on spindle-bead microfibers has confirmed the significant effect of cavity beads on increasing the water collection efficiency *via* a single fiber.[191,205] A specially designed structure of a single fiber produces controlled surface roughness, mechanical strength, and wetting properties,[206,207] as shown in Fig. 6. The droplet adhesion ability is better on geometrically designed thin fibers with beads than on smooth fibers.[192,208] The special structure enables droplets to adhere more strongly to fibers with beads: something which is also dependent on the different tilt angles of the fiber.[209] Moreover, droplets move toward beads and coalesce together.[193,210,211] Such fibers are able to accumulate larger droplets, so the fibers have longer contact with water, which often results in a more effective way of catching droplets.[212]

Surface geometry and differences in wettability play a key role in the generation of Laplace pressure. The pressure difference at the boundary between the gas and liquid phases occurs at surface bumps[213] and is determined as:

$$\Delta P = -\int_{r_1}^{r_2} \frac{2\gamma}{(r+R)^2}\sin\beta \, dz \qquad (1)$$

where γ is the water surface tension, r is the fiber local radius, R is the droplet radius, β is the half apex-angle of the bead, z is the integrating variable along the diameter of the bead.[22,214]

The Laplace pressure affects water collection on spider fibers covered with sticky glue beads, which are a more wettable region than hydrophobic threads[22] and water droplets maintain the spherical shape due to the surface tension.[207,214,215] Importantly, nano and microstructures at the surfaces increase the Laplace pressure gradient. Therefore, water droplet collection on the fibers with beads, where gradients of the Laplace pressure occur, significantly affects the wettability of fibers. The droplet formed on a bead has a different radius than that formed on a smooth fiber. The pressure in the droplet formed on the fiber is greater than the pressure in the droplet on the bead due to the fiber's larger curvature. Consequently, it results in a nonequilibrium pressure difference, which causes directional movement of the droplet towards the bead on the fiber.

Wetting of meshes: hydrophilic *versus* hydrophobic properties

Generally speaking, water collection rates are affected by the wetting properties of the meshes. The mechanism of water droplet collection was studied by Zhang *et al.*[216] on superhydrophobic silica microfibers with a carbon nanoparticle
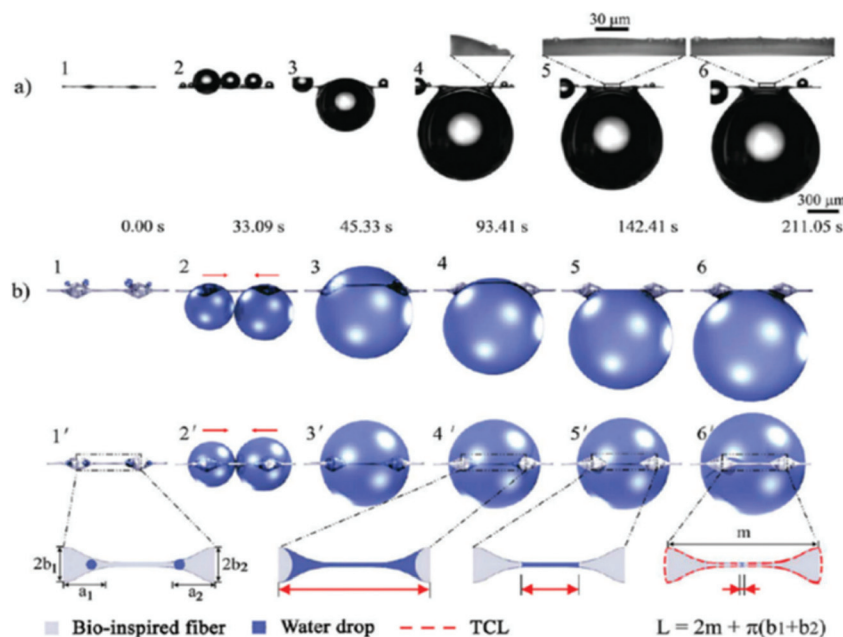
Fig. 6 Water collection on a two-spindle bead fiber: (a) optical image and (b) model illustration. Adapted and reproduced with permission.[207]

coating and an average diameter of 150 μm. A significant difference in effective water collection between coated and uncoated fibers was observed, as the water contact angle for superhydrophobic coated microfibers was 152°, while it was hydrophilic for the uncoated material, arriving at only 35°. Water droplets on the coated superhydrophobic fiber took on a hanging clamshell shape: one that grows and coalesces together until it finally falls down. Conversely, hydrophilic uncoated fibers collected droplets that were barrel-shaped, holding the droplets on their surface longer than the superhydrophobic fibers did. This eventually led to two-fold higher water collection efficiency for the coated silica microfibers than for the uncoated ones. Interestingly, the changing of the tilting angle from the horizontal position to 30° in 5° steps almost increased the amount of water collected because the droplets slid along the fiber, which increased their falling frequency. Dong *et al.*[217] used fibers from artificial spider silks (with an average diameter of ≈18 μm) to prove the importance of the angles between two adjacent fibers in fog collection efficiency. The highest water collection efficiency was achieved when the angle between the two fibers was 30°.

Hydrophobic and hydrophilic meshes are characterized by a different droplet sliding system, as shown in Fig. 7. Droplets collected on the hydrophobic mesh run down faster than they do on the hydrophilic one.[161] In another case, to accelerate droplet sliding from the meshes, the hydrophilic fraction of PA6 nanofibers was added to the hydrophobic PS microfibers, as indicated in the schematics in Fig. 8a and b. The contact angle hysteresis was reduced as the surface roughness of the PS microfibers was also reduced by adding the PA6 nanofibers. Thus, the water collection process was improved, obtaining the highest efficiency in water collection with PS-PA6 composite

meshes.[125] Hydrophilic surfaces are more effective in the condensation of water droplets, as indicated in many examples in the nature,[171] where droplets rollover from the meshes with hydrophobic properties.[218] The surface architecture and chemistry created by a hydrophobic matrix with hydrophilic domains were copied using hydrophilic chitosan (CS) islands attached to the hydrophobic surface of PVDF membranes for desalination[219] and water purification processes.[220]

The wetting of individual fibers or wires differs in comparison to the network of fibers or meshes. On individual fibers, the water droplet grows only until the adhesion forces are unable to hold it any longer. The growing water droplets on meshes get in contact with more fibers, thereby increasing the droplet–surface contact area, and it needs more time to run down freely from the vertical mesh. Also, on hydrophilic meshes larger agglomerates of water droplets tend to remain between the fibers, which inhibits the fog flow through the mesh, reducing the water collection efficiency. Despite the decrease in the fog collection rate caused by blockage of pores, the mesh has a sufficiently larger collection area and by keeping them hydrophobic, it will still collect more water than individual fibers. The wetting properties of the mesh affect both the ability to capture droplets and the mechanism of their removal from the surface. The size of the droplets shown in Fig. 7 is the result of the capture of small water droplets by the mesh and their coalescence together.

Current limitations in understanding wetting behavior at fibrous arrays are often due to the use of wetting theories, such as Wenzel[221] and Cassie-Baxter,[222] that do not fully consider the geometry of the wetted surface.[223–225] However, the work by Duprat *et al.*[195] has used a description of capillary force applied to fiber arrays from Princen *et al.*[226] to derive an
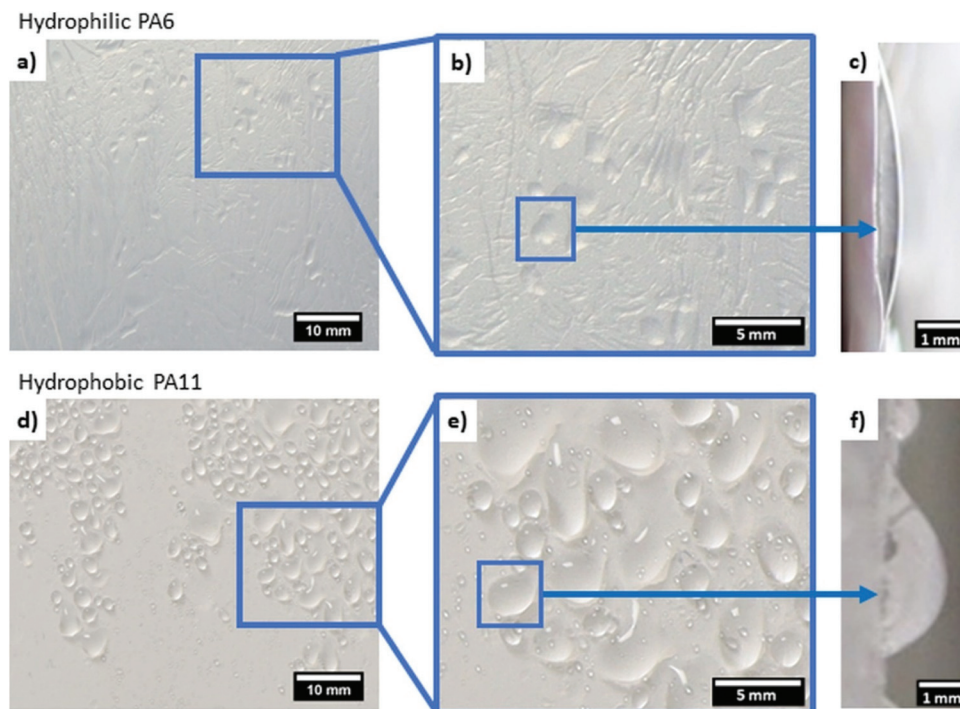
Fig. 7 Comparing the shape of droplets collected on the electrospun (a–c) hydrophilic PA6 and (d–f) hydrophobic PA11 meshes. Adapted and reproduced with permission.[161]
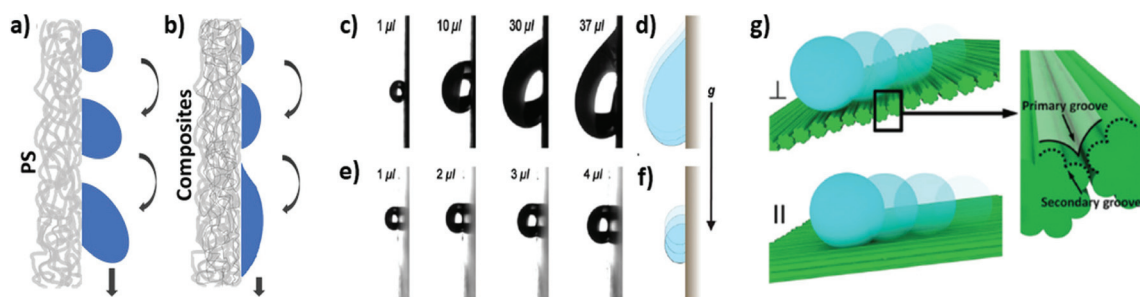

Fig. 8 Schematics of water droplets moving down on an electrospun: (a) hydrophobic PS microfiber mesh; (b) PS-PA6 composite mesh with hydrophobic PS microfibers and hydrophilic PA6 nanofibers; (c,d) PVDF-HFP fibrous nanomats; (e,f) PVDF-HFP fibrous nanomats impregnated with total quartz oil; (g) on the double-grooved surfaces in different directions. Adapted and reproduced with permission.[125,165,184]

energy balance approach whereby the spreading of liquid lowers the energy of the system but also requires bending of the wetted fibers, which requires energy. Importantly, it suggested the main concept of liquids having a range of wetting behavior across different length scales. For instance, a liquid may spread at a solid fiber surface whereas a liquid droplet, of considerably greater size than the liquid–fiber interface, may exhibit non-spreading behavior.

Permeability

The permeability of the meshes used for collecting fog droplets is another crucial parameter for tuning the water harvesting efficiency. The pores in meshes can be clogged by the accumulated water that has not drained, thus obstructing the space for catching more droplets from the air.[31,36,37,227] To increase

the permeability of the nanofiber-based meshes, characterized by a pore size of 1 μm or smaller,[228] the important part is the incorporation of hydrophobic elements, thus permitting much faster water drainage from the meshes.[161] The comparison between the hydrophilic PA6 and hydrophobic PA11 shows that the drainage system for hydrophobic meshes is more effective, while the water collected is not reducing the permeability of the mesh for the further water collection process.

5. Designs of fog water collectors with electrospun fibers

The continuous development and studies of various designs of fog collector meshes in the past decade are shown in Table 1

Table 1 Comparison of different fiber meshes and their water collection rate, including the experimental parameters used in the literature

References	Polymer mesh	Average fiber diameter [μm]	Water contact angle [°]	Water collection rate [mg cm^{-2} h^{-1}]	Fog collection parameters
Almasian et al.[229]	PAN nanofibers	0.08	106	31	Conventional humidifier; fog flow velocity: 0.60 cm s^{-1}; distance: 15 cm; tilting angle: 90°; environmental conditions: T = 20 °C; RH = 70%; and collection time: 1 h
	Fluorinated-PAN nanofibers	0.09	159	335	
Azad et al.[163]	PET fibers with profile widths smaller than 1 mm	—	78 ± 2	~1.10–2.15 mg per 30 min	Ultrasonic humidifier (Honeywell, BH-860E); fog flow velocity: ~1.6 m s^{-1}; distance: 17 cm; tilting angle: 90°; environmental conditions: T = 19–20 °C; RH = 75–85%; and collection time: 30 min
	PET fibers with profile widths larger than 1 mm	—		~0.95–1.40 mg per 30 min	
Bai et al.[231]	Single artificial cactus spine cover by nanogrooved PI fibers	—	—	~0.30 μL min^{-1}	Ultrasonic humidifier; (Goal, G0-2028, China); fog flow velocity: 55–60 cm s^{-1}; distance: 4 cm; tilting angle: 90°, 45°, 0°, −45°, and −90°; environmental conditions: room temperature; and collection time: 15 min
Ganesh et al.[235]	PVDF-HFP-FPOSS neat nanofibers	0.65 ± 0.03	145 ± 2	63	Conventional humidifier; fog flow velocity: >40 cm s^{-1}; distance: 5 cm; tilting angle: 45°; environmental conditions: T = 23 °C; RH = 70%; and collection time: 1 h
	PVDF-HFP-FPOSS nanofibers with microparticles	0.61 ± 0.04	147 ± 2	69	
	PVDF-HFP-FPOSS nanofibers with hierarchical structures	0.14 ± 0.02 for nanopillars	153 ± 2	81	
Hu et al.[215]	Membrane from anodized Cu with PVDF-HFP nanofibers electrospun for	—	141 ± 1 (PVDF fibers) ~ 0 (hybrid membrane)		Unknown humidifier; fog flow velocity: 7.262 g min^{-1} cm^{-2}; distance: —; tilting angle: —; environmental conditions: —; and collection time: —
	1 min			~42	
	3 min			~72	
	5 min			116	
	7 min			110	
Knapczyk-Korczak et al.[125]	PS fibers	4.80 ± 0.22	142 ± 2	45	Conventional humidifier (Beurer GmbH, Germany); fog flow velocity: 0.19 m s^{-1}; distance: 15 cm; tilting angle: 30°; environmental conditions: T = 30 °C; RH = 95%; and collection time: 3 h
	PA6 fibers	0.11 ± 0.03	45 ± 2	29	
	PS(1)-PA6(4)	4.80 ± 0.22 (PS); 0.11 ± 0.03 (PA6)	123 ± 2	43	
Knapczyk-Korczak et al.[126]	PS fibers	4.80 ± 0.22	142 ± 2	56	Distance: 6 cm; and tilting angle: 90°
	CA fibers	0.54 ± 0.16	127 ± 3	59	Conventional humidifier (Beurer GmbH, Germany); fog flow velocity: 0.19 m s^{-1}; distance: 6 cm; tilting angle: 90°; environmental conditions: RH = 95%–99%; and collection time: 3 h
	Side-by-side PS-CA fibers	1.75 ± 0.27	153 ± 4	45	
				71	
Knapczyk-Korczak and Szewczyk et al.[233]	Commercial Raschel mesh	1610 ± 120	90 ± 4	21	Conventional humidifier (Beurer GmbH, Germany); fog flow velocity: 0.19 m s^{-1}; distance: 6 cm; tilting angle: 90°; environmental conditions: RH = 95%–99%; and collection time: 3 h
	Random PVDF fibers	1.29 ± 0.34	140 ± 6	35	
	Aligned PVDF fibers	1.48 ± 0.28	124 ± 6 parallel; 118 ± 4 perpendicular	51	
	Raschel + random PVDF fibers	2.14 ± 0.78	—	64	
	Raschel + aligned PVDF fibers	1.49 ± 0.36	—	53	
Knapczyk-Korczak et al.[234]	PA6 nanofibers	0.11 ± 0.03	45 ± 2	43	Conventional humidifier (Beurer GmbH, Germany); fog flow velocity: 0.19 m s^{-1}; distance: 6 cm; tilting angle: 90°; environmental conditions: RH = 95%–99%; and collection time: 3 h
	Raschel + PA6 nanofibers	0.12 ± 0.02	—	65	
Lalia et al.[184]	Unimpregnated PVDF-HFP nanomats	0.10 to 0.50	134 ± 4	88 ± 4	Conventional ultrasonic humidifier (Joycare Italy); fog flow velocity: 40 cm s^{-1}; distance: 6 cm; tilting angle: 45°; environmental conditions: T = 20 °C; RH = 70%; and collection time: 1 h
	Impregnated PVDF-HFP nanomats with total quartz oil		94 ± 4	100 ± 5	
	Impregnated PVDF-HFP nanomats with Krytox-1506 oil		116 ± 4	118 ± 6	

Table 1 (Contd.)

References	Polymer mesh	Average fiber diameter [μm]	Water contact angle [°]	Water collection rate [mg cm⁻² h⁻¹]	Fog collection parameters
Liang et al.[165]	Single-grooved (parallel)	~0.20	129	2.8 ml	Unknown humidifier; fog flow velocity: ~60 cm s⁻¹, distance: —; tilting angle: 20°; environmental conditions: —; and collection time: —
	Double-grooved (parallel)	~0.90	145	1.1 ml	
	Double-grooved (perpendicular)			4.2 ml	
Shigezawa et al.[232]	Nylon mesh	100	—	~185	Conventional humidifier; fog flow velocity: —; distance: —; tilting angle: 90°; environmental conditions: T = 20 °C; RH = 70%; and collection time: 2 h
	Nylon mesh covered by CA – 1 min	1.70 for CA	—	~390	
Thakur et al.[214]	Neat PNIPAM	0.22 ± 0.06	3 ± 1 (25 °C); 81 ± 2 (40 °C)	~650 (25 °C); 401 ± 13 (40 °C)	Conventional humidifier; fog flow velocity: —; distance: 7 cm; tilting angle: 45°; environmental conditions: T = 25 and 40 °C; RH = 70%; and collection time: 1 h
	Neat PVDF	0.49 ± 0.145	131 ± 1 (25 °C, 40 °C)	600 ± 18 (25 °C); 532 ± 17 (40 °C)	
	Hydrophilic–hydrophobic PNIPAM-PVDF	String: 0.72 ± 0.03; spindle bead: 14 ± 2 (length), 9 ± 2 (diameter)	26 ± 1 (25 °C); 101 ± 2 (40 °C)	1150 ± 28 (25 °C); 909 ± 31 (40 °C)	
Uddin et al.[230]	PAN/PMMA without nanoparticles (NP)	0.47	131	258	Conventional ultrasonic humidifier (Vicks, USA); fog flow velocity: 330 ml h⁻¹; distance: 5 cm; tilting angle: 90°; environmental conditions: T = 19 ± 2 °C; RH = 68 ± 3%; and collection time: 1 h
	PAN/PMMA/2.5 wt% NP	—	~142	411	
	PAN/PMMA/5 wt% NP	—	~150	507	
	PAN/PMMA/10 wt% NP	1.30	155	621	
Ura et al.[156]	PC(+) 25%	2.27 ± 0.48	112 ± 4	65	Conventional humidifier; (Beurer GmbH, Germany); fog flow velocity: 0.19 m s⁻¹; distance: 6 cm; tilting angle: 90°; environmental conditions: RH = 95%–99%; and collection time: 3 h
	PC(−) 25%	2.33 ± 0.51	125 ± 4	76	
	PC(+) 40%	2.78 ± 0.54	112 ± 3	69	
	PC(−) 40%	2.77 ± 0.43	118 ± 4	78	

with summaries of how their efficiency was tested. Thakur et al.[214] used Bead-On-String Hierarchical Fibers obtained via core–shell electrospinning. The combination of hydrophilic PNIPAM (poly(N-isopropylacrylamide)) and hydrophobic PVDF in hierarchical fibrous structures successfully mimics the natural spider silk with spindle-bead geometry. This special combination of hydrophobic fibers with hydrophilic beads demonstrated the applicability of core–shell fibers for fog collection. Moreover, the authors proved the influence of ambient temperature in effective fog collection. When the temperature in the chamber was increased from 25 to 40 °C, the fog collection efficiency decreased due to increased droplet evaporation, as shown in Fig. 9a. Electrospun PVDF-HFP nanomats were used by Lalia et al. to catch water from fog[184] The water collection rate for unimpregnated nanomats was 77 mg cm⁻² h⁻¹ for the water collected from the mesh and 11 mg cm⁻² h⁻¹ for the water retained in the mesh. The modified nanomats impregnated with Krytox-1506 oil collected 118 mg cm⁻² h⁻¹ of water from the mesh. The diameter of the fibers ranged from 100 nm to 500 nm and created a porous structure with a rough surface. The fog flow velocity and the distance between the mesh and humidifier output, which were less than 40 cm s⁻¹ and 6 cm, respectively, had a significant effect on fog collection. Moreover, the impregnation of nanomats with special oils affected the droplet sliding mechanism, as shown in Fig. 8c–f. Electrospun hydrophobic poly(vinylidene fluoride-co-hexafluoropropylene) (PVDF-HFP) nanofibers were used with a hydrophilic nanoneedle copper mesh by Hu et al.[215] The prepared hybrid composite with randomly oriented PVDF-HFP fibers was electrochemically oxidized. Cu mesh was electrochemically anodized, thus making it possible to obtain a layer of $Cu(OH)_2$ nanoneedles which started to grow from Cu wires. This modification, based on the use of electrospun fibers, allowed to achieve a fog collection efficiency of 0.116 g min⁻¹ cm⁻². As the wettability of materials determines the fog harvesting possibility, electrospun polyacrylonitrile (PAN) nanofibers were modified by immersion in a special solution containing 2-propanol, deionized water, fluoroamine compound, and potassium carbonate as a catalyst. The obtained coating resulted in a higher water contact angle, 159° on the fluorinated PAN nanofibers, than the 106° on the unmodified PAN nanofibers.[229] Uddin et al.[230] electrospun nanocomposite fibers from PAN and poly(methyl methacrylate) (PMMA) with the addition of Al and TiO_2 micro- and nanoparticles, and carbonized them, producing composites with combined superhydrophobic–hydrophilic properties. The fabricated mesh with 10 wt% of nanoparticle inclusions achieved the highest average roughness, appearing superhydrophobic. This combination of superhydrophobic–hydrophilic properties in nanocomposite fibers significantly affects fog water harvesting. The addition of hydrophilic TiO_2 nanoparticles was crucial for the adhesion and fixing of water droplets, which rolled down the superhydrophobic fibers effectively.

Apart from chemical coatings, the changes in electrospun fiber morphology affect their wetting properties.[144] Azad et al.[163] tested 14 different PET fiber profiles to collect water
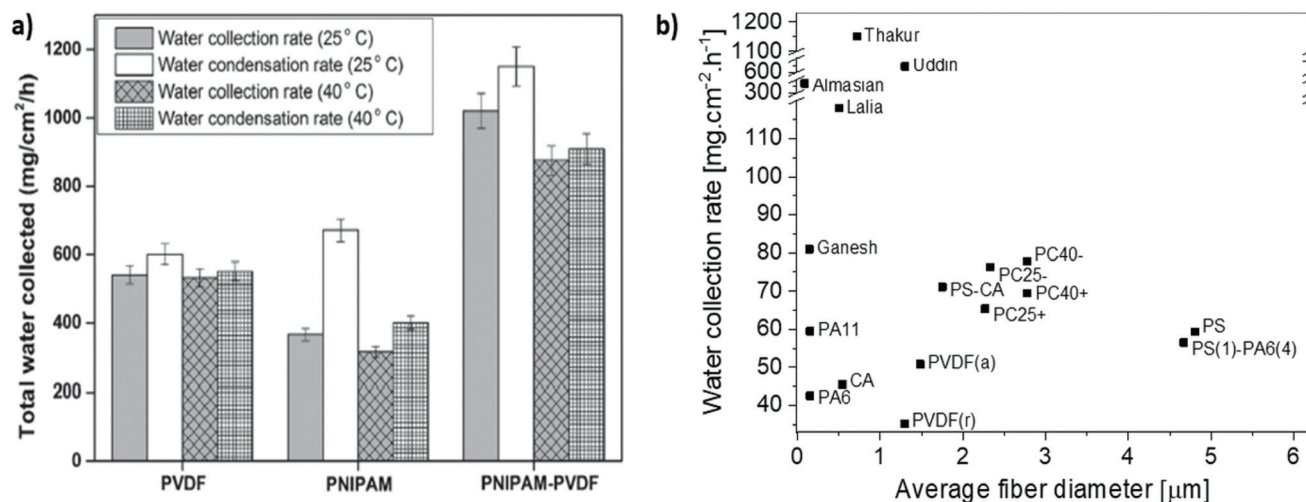
Fig. 9 Comparison of the water collection rate by various electrospun meshes (a) at different temperatures – adapted and reproduced with permission;[214] (b) with different average diameters of fibers – data taken from the following references: Lalia *et al.*,[184] Thakur *et al.*,[214] Almasian *et al.*,[229] Uddin *et al.*,[230] and Ganesh *et al.*[235]

from fog. They had a width between 317 and 2300 μm and were grouped into profiles with widths smaller and larger than 1 mm. Fiber samples used for fog collection differed in shape and cross-sectional view, but fibers covered nearly 55% of the area, and the fog could flow freely through. The best water collection rate was obtained for microgrooved surfaces with a rectangular cross-section with round edges (∼2100 μg per 30 min) and smooth surfaces with an oval cross-section (∼1750 μg per 30 min). In another study, the wrinkled PI fibers mimicked artificial cactus spines.[231] To obtain their special designs, bare silver needles were covered with electrospun PAA-PS composite fibers, which were turned into nanogrooved PI fibers by thermal imidization treatment. Water collection was demonstrated on a model equipped with 180 artificial spines placed on a spherical sponge. This cactus model collected 1.3 mL of water in 15 min, with the water collection rate for a single spine estimated to be 0.3 μL min^{-1}. Liang *et al.*[165] measured the effect of grooved and double-grooved fiber structures on fog collection ability, as shown in Fig. 8g. Double-grooved fibers from poly(L-lactic acid) (PLLA) oriented parallel to the direction of flowing droplets collected greater amounts of water than single-grooved fibers.

In addition, the combination of fibers of different sizes is crucial for effective water harvesting. Shigezawa *et al.*[232] investigated a fiber-based system to collect water inspired by *Berkhera purpurea* hairs. This amazing plant system combines thick hydrophobic hair (60–80 μm) with thin hydrophilic fibers (3–8 μm). To imitate this unique system, a nylon mesh (Muramatu K601, from Muramatu Co. Ltd Japan) was covered with electrospun cellulose acetate (CA) fibers with different put times (10 s, 1 min, 5 min, 10 min). The highest water collection efficiency was obtained for the sample CA-1 min because of the controlled size of the void, which provided an easy way to drain droplets into the beaker (Fig. 10). Another approach to efficient water harvesting is to modify existing FWCs with elec-

trospun fibers.[233,234] The simple incorporation of PVDF and PA6 fibers into a commercial Raschel mesh in the electrospinning process increased its water collection rate by 300%. PS-PA6 composites showed a similar system based on hydrophobic PS microfibers and hydrophilic PA6 nanofibers.[125] However, the composites obtained had a different structure from that of the *Shigezawa*[232] materials and did not have voids. These electrospun meshes are filled with fibers, but their structure has a high number of pores, resulting in their high permeability. The addition of PA6 nanofibers to PS microfibers reduces the blockage of pores. These combinations created effective water drainage from the mesh, and collection on the thicker hydrophobic fibers.

6. Summary of the key points of fog collection parameters and recommendations

The comparison of fog water collection results is challenging due to the differences in experimental set-ups, parameters, and conditions (Table 1). As shown in Fig. 9, many differences in the experimental parameters, such as fog flow velocity or distance between the humidifier outlet and mesh, have a direct effect on water collection results. Importantly, the type of humidifier and also the change in the fog flow velocity and droplet size are crucial for an appropriate water collection study when mimicking fog under laboratory conditions. In Table 2 we compared the most important parameters in fog water collection under laboratory conditions. This comparison was based on the literature discussed previously in sections 4 and 5 and makes it possible to standardize the laboratory-scale experiments of fog collection. In Fig. 11, the graphic summary indicates the key elements to keep in mind when
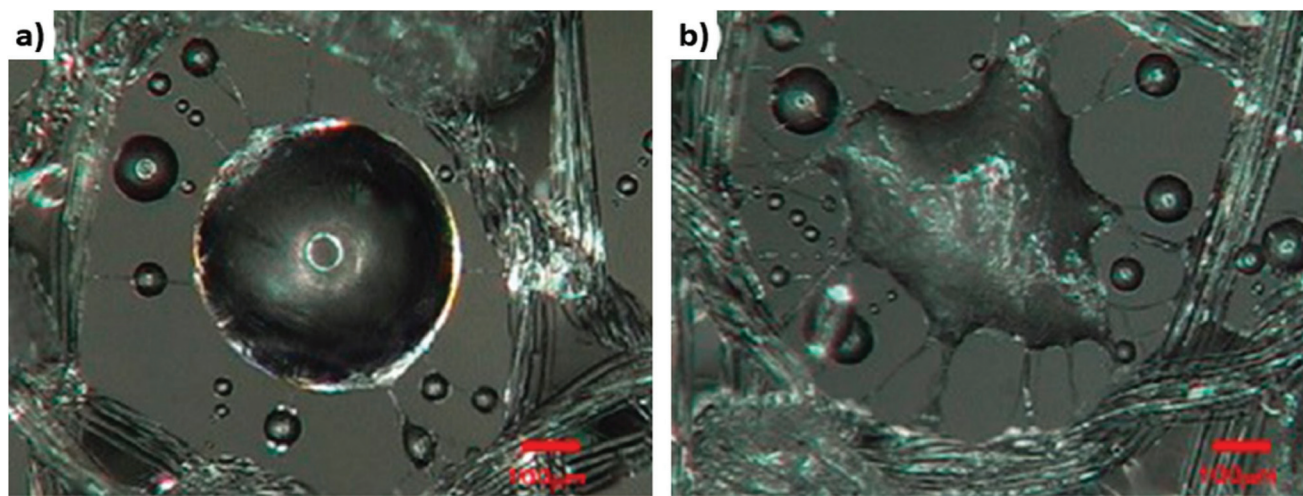
Fig. 10 The water droplets collected on CA fibers electrospun on nylon mesh in (a) 1 min and (b) 5 min. Adapted and reproduced with permission.[232]

Table 2 The summary of the key parameters in fog water collection experiments performed at the laboratory scale

Parameters	Effect on the experimental result
Humidifier	
Type of humidifier (vapor or ultrasonic)	• The ultrasonic humidifier produces fog, whereas the vapor humidifier creates vapor • The vapor humidifier produces droplets much smaller than fog droplets, thus lowering the water collection rate • The droplets produced from vapor humidifiers need to condense to create fog
Fog flow velocity and humidifier efficiency	• The effectiveness of fog collection depends on the humidifier's fog production efficiency • The fog flow velocity significantly affects the number of fog droplets passing through the mesh • A high efficiency of the humidifier and high fog flow velocity can significantly increase water collection
Collection parameters	
Distance between the mesh and humidifier output	• The water collection rate increases when reducing this distance, because the fog passing through the mesh has a higher concentration of droplets (higher fog density, less diluted fog)
Humidity	• Affects the evaporation of small droplets from the mesh before they flow down
Ambient temperature	• High temperature accelerates the evaporation of the passing and captured droplets, which reduces the water collection rate
Collection time	• The droplets start to run down or roll off only when they reach the critical volume of accumulation in the mesh • Setting the right collection time, in relation to the water saturation of the mesh, is important
Mesh construction	
Size and thickness	• The fog should pass through the entire surface of the mesh • The mesh thickness significantly affects permeability • A mesh that is too thick can decrease the fog collection rate
Permeability of meshes	• Affects the velocity of the fog flow passing through the mesh • In low permeability meshes, the blockage of pores by water is a problem • Depends on the fiber diameter and pore size of the mesh
Fiber diameter and pore size	• The accumulation of water droplets and the clogging of pores are related to the pore size • Pore size often depends on the fiber diameter and fiber arrangement in the mesh

designing an experimental set-up, in order to facilitate comparisons among various fog water harvesting studies.

The efficiencies of the fog collection of various systems based on polymer fibers were compared using the water collection rates expressed in mg cm^{-2} h^{-1}. This unit provides information of the water collected amount per unit area and it refers to the collection time, which is needed for comparison of efficient water collection in various systems. The collected water can be measured both by weight and by volume. Relatively small amounts of water are obtained at the labora-

tory scale, compared to the research conducted in the field studies, and therefore often the weight of the obtained water is used. The water collected by commercial meshes is usually expressed in L m^{-2} day^{-1} due to the much larger scale. In the literature, the effectiveness of the fog water collection, *e.g.* water collection rate, is often called collection efficiency or collection performance, which is misleading, because the efficiency has to be expressed as a fraction or percent. The use of the above terms is correct if we do not provide specific values expressed in units determining, *e.g.*, the water collection rate.
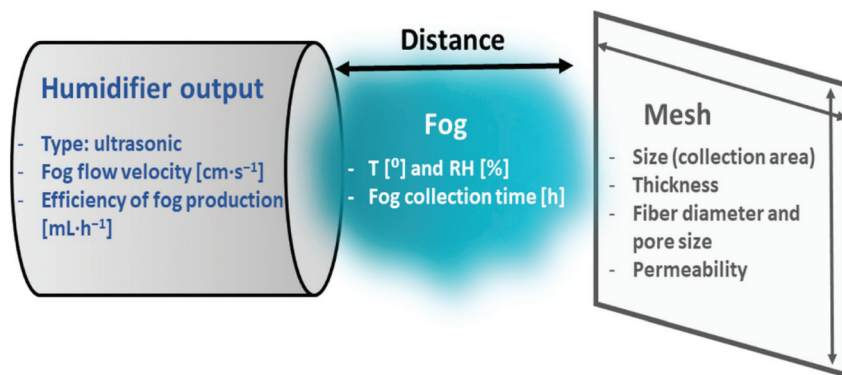
Fig. 11 The graphic illustration of the most important fog collection parameters in laboratory-scale experiments.

Obviously, fog collectors are effective in foggy regions, however, their effectiveness depends on the wind speed which pushes the fog through the mesh. The highest results obtained by commercial Raschel mesh are achieved when the wind speed reaches 1–2 m s^{-1}.[33] Systems containing nano- and microfibers significantly increase the water collection area. Also the high porosity of the electrospun membranes retains high permeability for the passing fog.[36,126,233,236] Importantly, these nanofiber based solutions are desired in the water collection under low wind conditions. Additionally, the efficiency of meshes under such conditions depends on the amount of water contained in the fog and the fast drainage system of water droplets to the container.

By all means, the stability of polymers used in FWC systems depends on the polymer structure and the mechanical characteristics of electrospun membranes. The selection of the polymer strictly depends on the requirements of its resistance to atmospheric and chemical factors. The biodegradation importance for the waste management issue and environmentally friendly aspects should be taken into account in the FWC designs as well. As mentioned above the weather conditions limit the effectiveness of FWCs. Electrospun nanofibers help in capturing more water, especially under low fog and wind conditions. Strong winds are known for damaging FWCs, and electrospun meshes. However, electrospun fibers can be easily deposited even in the field of portable electrospinning devices, currently used in wound care.[237]

7. Conclusions

Water harvesting continues to be a global challenge. Nano- and micropolymer webs with unique fiber structures open new paths in fog water droplet collection. In particular, electrospun polymer fibers have great potential in water harvesting. The versatility of production methods makes it possible to combine hydrophobic and hydrophilic properties, which are desirable for effective water collection. Moreover, their mechanical properties also provide wind resistance, especially when they are combined with the existing FWC technologies already available on the market. This review compares the fog water collection efficiency in structures based on nano- and microfibers. Importantly, we included the guidelines for testing the new design meshes at the laboratory scale and indicated the most important parameters to be considered for testing FWC before field studies. The reviewed literature reveals the current strategies used in designing spider web-inspired biomimetic meshes to collect water effectively, paving the way for the future development of new fog collector systems. FWCs are excellent examples of a bioinspired and sustainable technology that is evolving continuously to meet critical water harvesting challenges. However, the functional outcomes of existing meshes used in collectors need improvement as many studies show the inadequacies in the engineering of surface microstructure and property designs. The ideal experimental conditions in fog collection research should include a precise position of the mesh in the fog stream, allowing the fog to flow through the entire mesh. The relative humidity close to the mesh region should approach 100%, as the reduction of humidity around the mesh can decrease the process efficiency due to a reduction in the water content in the fog. Moreover, the obtained results of water captured in fog collectors should be always calculated per area of mesh and collection time.

Conflicts of interest

Authors declare no conflict of interest.

Acknowledgements

References

1 R. Bagatin, J. J. Klemeš, A. Pietro Reverberi and D. Huisingh, *J. Cleaner Prod.*, 2014, **77**, 1–9.

2 G. Konapala, A. K. Mishra, Y. Wada and M. E. Mann, *Nat. Commun.*, 2020, **11**, 1–10.

3 J. Yu, J. Zhou, A. Long, X. He, X. Deng and Y. Chen, *Int. J. Environ. Res. Public Health*, 2019, **16**, 1–19.

4 B. Bhushan, *Philos. Trans. R. Soc., A*, 2020, **378**, 20190440.

5 P. S. Brown and B. Bhushan, *Philos. Trans. R. Soc., A*, 2016, **374**, 20160135.

6 B. Bhushan, *Philos. Trans. R. Soc., A*, 2019, **377**, 20190119.

7 D. Gurera and B. Bhushan, *Philos. Trans. R. Soc., A*, 2020, **378**, 20190444.

8 L. T. Nguyen, Z. Bai, J. Zhu, C. Gao, X. Liu, B. T. Wagaye, J. Li, B. Zhang and J. Guo, *ACS Omega*, 2021, **6**, 3910–3920.

9 P. Comanns, F. J. Esser, P. H. Kappel, W. Baumgartner, J. Shaw and P. C. Withers, *R. Soc. Open Sci.*, 2017, **4**, 170591.

10 A.-C. Joel, G. Buchberger and P. Comanns, *Functional Surfaces in Biology III*, Springer International Publishing, Cham, 2017, vol. 10.

11 J. Ju, H. Bai, Y. Zheng, T. Zhao, R. Fang and L. Jiang, *Nat. Commun.*, 2012, **3**, 1246–1247.

12 F. T. Malik, R. M. Clement, D. T. Gethin, M. Kiernan, T. Goral, P. Griffiths, D. Beynon and A. R. Parker, *Philos. Trans. R. Soc., A*, 2016, **374**, 20160110.

13 Y. Xue, T. Wang, W. Shi, L. Sun and Y. Zheng, *RSC Adv.*, 2014, **4**, 40837–40840.

14 R. Feng, F. Song, C. Xu, X.-L. Wang and Y.-Z. Wang, *Chem. Eng. J.*, 2021, **422**, 130119.

15 H. Geng, Q. Xu, M. Wu, H. Ma, P. Zhang, T. Gao, L. Qu, T. Ma and C. Li, *Nat. Commun.*, 2019, **10**, 1–10.

16 Y. Gu, L. Yu, J. Mou, D. Wu, P. Zhou and M. Xu, *e-Polym.*, 2020, **20**, 443–457.

17 Y. Zhao, K. T. T. Hien, G. Mizutani and H. N. Rutt, *Appl. Phys. B: Lasers Opt.*, 2017, **123**, 188.

18 F. Vollrath and D. T. Edmonds, *Nature*, 1989, **340**, 305–307.

19 G. R. Plaza, G. V. Guinea, J. Pérez-Rigueiro and M. Elices, *J. Polym. Sci., Part B: Polym. Phys.*, 2006, **44**, 994–999.

20 J. E. Garb, R. A. Haney, E. E. Schwager, M. Gregorič, M. Kuntner, I. Agnarsson and T. A. Blackledge, *Commun. Biol.*, 2019, **2**, 275.

21 X. Liu, L. Shi, X. Wan, B. Dai, M. Yang, Z. Gu, X. Shi, L. Jiang and S. Wang, *Adv. Mater.*, 2021, **33**, 2007301.

22 Y. Zheng, H. Bai, Z. Huang, X. Tian, F. Q. Nie, Y. Zhao, J. Zhai and L. Jiang, *Nature*, 2010, **463**, 640–643.

23 H. Jarimi, R. Powell and S. Riffat, *Int. J. Low-Carbon Tech.*, 2020, **15**, 253–276.

24 S. Sharifvaghefi and H. Kazerooni, *SN Appl. Sci.*, 2021, **3**, 516.

25 D. Gurera and B. Bhushan, *J. Colloid Interface Sci.*, 2020, **560**, 138–148.

26 İ. A. Kariper, *npj Clean Water*, 2021, **4**, 24.

27 K. Lucier and M. Qadir, *Water*, 2018, **10**, 1472.

28 R. S. Schemenauer and P. Cereceda, *Ambio*, 1991, **20**, 303–308.

29 R. S. Schemenauer and P. Cereceda, *J. Appl. Meteorol.*, 1994, **33**, 1313–1322.

30 J. de D. Rivera and D. Lopez-Garcia, *Atmos. Res.*, 2015, **151**, 250–258.

31 R. Holmes, J. de D. Rivera and E. de la Jara, *Atmos. Res.*, 2015, **151**, 236–249.

32 O. Klemm, R. S. Schemenauer, A. Lummerich, P. Cereceda, V. Marzol, D. Corell, J. Van Heerden, D. Reinhard, T. Gherezghiher, J. Olivier, P. Osses, J. Sarsour, E. Frost, M. J. Estrela, J. A. Valiente and G. M. Fessehaye, *Ambio*, 2012, **41**, 221–234.

33 D. M. Fernandez, A. Torregrosa, P. S. Weiss-Penzias, B. J. Zhang, D. Sorensen, R. E. Cohen, G. H. McKinley, J. Kleingartner, A. Oliphant and M. Bowman, *Aerosol Air Qual. Res.*, 2018, **18**, 270–283.

34 R. S. Schemenauer and P. Cereceda, *Water Int.*, 1994, **19**, 70–76.

35 S. Swarndeep, *Int. J. Innovative Sci., Eng. Technol.*, 2016, **3**, 623–629.

36 K. C. Park, S. S. Chhatre, S. Srinivasan, R. E. Cohen and G. H. McKinley, *Langmuir*, 2013, **29**, 13269–13277.

37 J. de D. Rivera, *Atmos. Res.*, 2011, **102**, 335–342.

38 M. Rajaram, X. Heng, M. Oza and C. Luo, *Colloids Surf., A*, 2016, **508**, 218–229.

39 A. Greiner and J. H. Wendorff, *Angew. Chem., Int. Ed.*, 2007, **46**, 5670–5703.

40 U. Stachewicz, I. Peker, W. Tu and A. H. Barber, *ACS Appl. Mater. Interfaces*, 2011, **3**, 1991–1996.

41 F. Zhang and A. H. Barber, *Macromol. Mater. Eng.*, 2017, **302**, 1–7.

42 I. Greenfeld, X. Sui and H. D. Wagner, *Macromolecules*, 2016, **49**, 6518–6530.

43 A. Arinstein and E. Zussman, *J. Polym. Sci., Part B: Polym. Phys.*, 2011, **49**, 691–707.

44 J. Yao, C. W. M. Bastiaansen and T. Peijs, *Fibers*, 2014, **2**, 158–187.

45 S. Metwally, J. E. Karbowniczek, P. K. Szewczyk, M. M. Marzec, A. Gruszczyński, A. Bernasik and U. Stachewicz, *Adv. Mater. Interfaces*, 2019, **6**, 1801211.

46 S. Agarwal, A. Greiner and J. H. Wendorff, *Prog. Polym. Sci.*, 2013, **38**, 963–991.

47 J. Xue, T. Wu, Y. Dai and Y. Xia, *Chem. Rev.*, 2019, **119**, 5298–5415.

48 Z. J. Krysiak, M. Z. Gawlik, J. Knapczyk-Korczak, L. Kaniuk and U. Stachewicz, *Materials*, 2020, **13**, 11–13.

49 Z. J. Krysiak, J. Knapczyk-Korczak, G. Maniak and U. Stachewicz, *Colloids Surf., B*, 2021, **199**, 111554.

50 D. Lv, M. Zhu, Z. Jiang, S. Jiang, Q. Zhang, R. Xiong and C. Huang, *Macromol. Mater. Eng.*, 2018, **303**, 1–18.

51 S. Ramakrishna, K. Fujihara, W. E. Teo, T. Yong, Z. Ma and R. Ramaseshan, *Mater. Today*, 2006, **9**, 40–50.

52 A. Gupta and S. R. Dhakate, in *Emerging Technologies for Nanoparticle Manufacturing*, Springer, Cham, 2021, pp. 203–236.

53 T. M. Subrahmanya, A. Bin Arshad, P. T. Lin, J. Widakdo, H. K. Makari, H. F. M. Austria, C.-C. Hu, J.-Y. Lai and W.-S. Hung, *RSC Adv.*, 2021, **11**, 9638–9663.

54 H. J. Jin, S. V. Fridrikh, G. C. Rutledge and D. L. Kaplan, *Biomacromolecules*, 2002, **3**, 1233–1239.

55 M. Wang, H. J. Jin, D. L. Kaplan and G. C. Rutledge, *Macromolecules*, 2004, **37**, 6856–6864.

56 N. Lin and B. Zuo, *J. Biomater. Sci., Polym. Ed.*, 2021, 1–15.

57 M. Ma, R. M. Hill and G. C. Rutledge, *J. Adhes. Sci. Technol.*, 2008, **22**, 1799–1817.

58 A. Tuteja, W. Choi, M. Ma, J. M. Mabry, S. A. Mazzella, G. C. Rutledge, G. H. McKinley and R. E. Cohen, *Science*, 2007, **318**, 1618–1622.

59 P. K. Szewczyk, D. P. Ura, S. Metwally, J. Knapczyk-Korczak, M. Gajek, M. M. Marzec, A. Bernasik and U. Stachewicz, *Polymer*, 2019, **11**, 34.

60 K. J. Kubiak, M. C. T. Wilson, T. G. Mathia and P. Carval, *Wear*, 2011, **271**, 523–528.

61 B. Bhushan, in *Biomimetics*, Springer, 2018, vol. 279, pp. 39–49.

62 M. Ma, M. Gupta, Z. Li, L. Zhai, K. K. Gleason, R. E. Cohen, M. F. Rubner and G. C. Rutledge, *Adv. Mater.*, 2007, **19**, 255–259.

63 U. Stachewicz, R. J. Bailey, H. Zhang, C. A. Stone, C. R. Willis and A. H. Barber, *ACS Appl. Mater. Interfaces*, 2015, **7**, 16645–16652.

64 S. Ramakrishna, K. Fujihara, W. E. Teo, T. Yong, Z. Ma and R. Ramaseshan, *Mater. Today*, 2006, **9**, 40–50.

65 C. J. Luo, S. D. Stoyanov, E. Stride, E. Pelan and M. Edirisinghe, *Chem. Soc. Rev.*, 2012, **41**, 4708–4735.

66 A. Walter, C. Westphal, P. Bliss and R. F. A. Moritz, *Behaviour*, 2011, **148**, 1297–1311.

67 S. Jalali, M. Aliabadi and M. Mahdavinejad, *Int. J. Build. Pathol. Adapt.*, 2021, DOI: 10.1108/ijbpa-01-2021-0007.

68 F. Vollrath, *Int. J. Biol. Macromol.*, 1999, **24**, 81–88.

69 I. Agnarsson, M. Kuntner and T. A. Blackledge, *PLoS One*, 2010, **5**, 1–8.

70 A.-C. Joel and W. Baumgartner, *J. Exp. Biol.*, 2017, **220**, 2243–2249.

71 O. Hakimi, D. P. Knight, F. Vollrath and P. Vadgama, *Composites, Part B*, 2007, **38**, 324–337.

72 A. C. Joel, P. Kappel, H. Adamova, W. Baumgartner and I. Scholz, *Arthropod Struct. Dev.*, 2015, **44**, 568–573.

73 D. Saravanan, *J. Text. Appar., Technol. Manag.*, 2006, **5**, 1–20.

74 S. J. Blamires, C. L. Wu, T. A. Blackledge and I. M. Tso, *J. R. Soc., Interface*, 2012, **9**, 2479–2487.

75 X. Hu, K. Vasanthavada, K. Kohler, S. McNary, A. M. F. Moore and C. A. Vierra, *Cell. Mol. Life Sci.*, 2006, **63**, 1986–1999.

76 K. N. Savage, P. A. Guerette and J. M. Gosline, *Biomacromolecules*, 2004, **5**, 675–679.

77 F. K. Ko and J. Jovicic, *Biomacromolecules*, 2004, **5**, 780–785.

78 O. Tokareva, M. Jacobsen, M. Buehler, J. Wong and D. L. Kaplan, *Acta Biomater.*, 2014, **10**, 1612–1626.

79 M. Xu and R. V. Lewis, *Proc. Natl. Acad. Sci. U. S. A.*, 1990, **87**, 7120–7124.

80 M. B. Hinman and R. V. Lewis, *J. Biol. Chem.*, 1992, **267**, 19320–19324.

81 T. Scheibel, *Microb. Cell Fact.*, 2004, **3**, 1–10.

82 D. Huemmerich, C. W. Helsen, S. Quedzuweit, J. Oschmann, R. Rudolph and T. Scheibel, *Biochemistry*, 2004, **43**, 13604–13612.

83 L. Eisoldt, A. Smith and T. Scheibel, *Mater. Today*, 2011, **14**, 80–86.

84 K. N. Savage and J. M. Gosline, *J. Exp. Biol.*, 2008, **211**, 1937–1947.

85 S. Singla, G. Amarpuri, N. Dhopatkar, T. A. Blackledge and A. Dhinojwala, *Nat. Commun.*, 2018, **9**, 1890.

86 H. Elettro, S. Neukirch, A. Antkowiak and F. Vollrath, *Sci. Nat.*, 2015, **102**, 2–5.

87 K. Kronenberger and F. Vollrath, *Biol. Lett.*, 2015, **11**, 2015–2018.

88 C. Belbéoch, J. Lejeune, P. Vroman and F. Salaün, *Environ. Chem. Lett.*, 2021, **19**, 1737–1763.

89 Y. Q. Zhang, *Biotechnol. Adv.*, 2002, **20**, 91–100.

90 K. Tsujimoto, H. Takagi, M. Takahashi, H. Yamada and S. Nakamori, *J. Biochem.*, 2001, **129**, 979–986.

91 B. D. Opell, *J. Arachnol.*, 2020, **48**, 278–283.

92 P. K. Szewczyk, J. Knapczyk-Korczak, D. P. Ura, S. Metwally, A. Gruszczyński and U. Stachewicz, *Mater. Lett.*, 2018, **233**, 211–214.

93 N. S. Paz and R. J. Raven, *J. Arachnol.*, 1990, **18**, 79–86.

94 Y. Yang, G. Greco, D. Maniglio, B. Mazzolai, C. Migliaresi, N. Pugno and A. Motta, *Mater. Sci. Eng., C*, 2020, **107**, 110197.

95 P. Szymkowiak, M. Tsiareshyna and R. Koczura, *Biologia*, 2020, **75**, 1679–1683.

96 A. Lazaris, S. Arcidiacono, Y. Huang, J. F. Zhou, F. Duguay, N. Chretien, E. A. Welsh, J. W. Soares and C. N. Karatzas, *Science*, 2002, **295**, 472–476.

97 X. Zhang, L. Xia, B. A. Day, T. I. Harris, P. Oliveira, C. Knittel, A. L. Licon, C. Gong, G. Dion, R. V. Lewis and J. A. Jones, *Biomacromolecules*, 2019, **20**, 2252–2264.

98 H. Wen, X. Lan, Y. Zhang, T. Zhao, Y. Wang, Z. Kajiura and M. Nakagaki, *Mol. Biol. Rep.*, 2010, **37**, 1815–1821.

99 F. Teulé, Y. G. Miao, B. H. Sohn, Y. S. Kim, J. J. Hull, M. J. Fraser, R. V. Lewis and D. L. Jarvis, *Proc. Natl. Acad. Sci. U. S. A.*, 2012, **109**, 923–928.

100 N. Nuraje, W. S. Khan, Y. Lei, M. Ceylan and R. Asmatulu, *J. Mater. Chem. A*, 2013, **1**, 1929–1946.

101 L. Shang, Y. Yu, Y. Liu, Z. Chen, T. Kong and Y. Zhao, *ACS Nano*, 2019, **13**, 2749–2772.

102 X. Shi, W. Zhou, D. Ma, Q. Ma, D. Bridges, Y. Ma and A. Hu, *J. Nanomater.*, 2015, **2015**, 1–20.

103 S. Agarwal, J. H. Wendorff and A. Greiner, *Polymer*, 2008, **49**, 5603–5621.

104 W. Wang, K. Ouaras, A. L. Rutz, X. Li, M. Gerigk, T. E. Naegele, G. G. Malliaras and Y. Y. S. Huang, *Sci. Adv.*, 2020, **6**, eaba0931.

105 T. Busolo, P. K. Szewczyk, M. Nair, U. Stachewicz and S. Kar-Narayan, *ACS Appl. Mater. Interfaces*, 2021, **13**, 16876–16886.

106 S. Jiang, Y. Chen, G. Duan, C. Mei, A. Greiner and S. Agarwal, *Polym. Chem.*, 2018, **9**, 2685–2720.

107 C. Wang, J. Wang, L. Zeng, Z. Qiao, X. Liu, H. Liu, J. Zhang and J. Ding, *Molecules*, 2019, **24**, 834.

108 Z. M. Huang, Y. Z. Zhang, M. Kotaki and S. Ramakrishna, *Compos. Sci. Technol.*, 2003, **63**, 2223–2253.

109 D. W. Hutmacher and P. D. Dalton, *Chem. – Asian J.*, 2011, **6**, 44–56.

110 D. H. Reneker and A. L. Yarin, *Polymer*, 2008, **49**, 2387–2425.

111 K. Garg and G. L. Bowlin, *Biomicrofluidics*, 2011, **5**, 013403.

112 M. M. Hohman, M. Shin, G. Rutledge and M. P. Brenner, *Phys. Fluids*, 2001, **13**, 2201–2220.

113 A. Kilic, F. Oruc and A. Demir, *Text. Res. J.*, 2008, **78**, 532–539.

114 S. Mahalingam, R. Matharu, S. Homer-Vanniasinkam and M. Edirisinghe, *Appl. Phys. Rev.*, 2020, **7**, 041302.

115 M. Gernhardt, L. Peng, M. Burgard, S. Jiang, B. Förster, H. Schmalz and S. Agarwal, *Macromol. Mater. Eng.*, 2018, **303**, 1–8.

116 L. Peng, S. Jiang, M. Seuß, A. Fery, G. Lang, T. Scheibel and S. Agarwal, *Macromol. Mater. Eng.*, 2016, **301**, 48–55.

117 Z. Sun, E. Zussman, A. L. Yarin, J. H. Wendorff and A. Greiner, *Adv. Mater.*, 2003, **15**, 1929–1932.

118 A. Greiner, J. H. Wendorff, A. L. Yarin and E. Zussman, *Appl. Microbiol. Biotechnol.*, 2006, **71**, 387–393.

119 S. A. Theron, E. Zussman and A. L. Yarin, *Polymer*, 2004, **45**, 2017–2030.

120 D. Li and Y. Xia, *Adv. Mater.*, 2004, **16**, 1151–1170.

121 N. T. Hiep and B. T. Lee, *J. Mater. Sci.: Mater. Med.*, 2010, **21**, 1969–1978.

122 D. Lovera, C. Bilbao, P. Schreier, L. Kador, H.-W. Schmidt and V. Altstädt, *Polym. Eng. Sci.*, 2009, **49**, 2430–2439.

123 J. W. Yoon, Y. Park, J. Kim and C. H. Park, *Fash. Text.*, 2017, **4**, 9.

124 X. Li, B. Ding, J. Lin, J. Yu and G. Sun, *J. Phys. Chem. C*, 2009, **113**, 20452–20457.

125 J. Knapczyk-Korczak, D. P. Ura, M. Gajek, M. M. Marzec, K. Berent, A. Bernasik, J. P. Chiverton and U. Stachewicz, *ACS Appl. Mater. Interfaces*, 2020, **12**, 1665–1676.

126 J. Knapczyk-Korczak, J. Zhu, D. P. Ura, P. K. Szewczyk, A. Gruszczyński, L. Benker, S. Agarwal and U. Stachewicz, *ACS Sustainable Chem. Eng.*, 2021, **9**, 180–188.

127 C. J. Luo, M. Nangrejo and M. Edirisinghe, *Polymer*, 2010, **51**, 1654–1662.

128 Z. Li and C. Wang, in *One-dimensional Nanostructures - Electrospinning Technique and Unique Nanofibers*, Springer Berlin Heidelberg, Berlin, Heidelberg, 2013, pp. 15–28.

129 P. K. Szewczyk and U. Stachewicz, *Adv. Colloid Interface Sci.*, 2020, **286**, 102315.

130 A. Haider, S. Haider and I.-K. Kang, *Arabian J. Chem.*, 2018, **11**, 1165–1188.

131 S. Huan, G. Liu, G. Han, W. Cheng, Z. Fu, Q. Wu and Q. Wang, *Materials*, 2015, **8**, 2718–2734.

132 T. Nitanan, P. Opanasopit, P. Akkaramongkolporn, T. Rojanarata, T. Ngawhirunpat and P. Supaphol, *Korean J. Chem. Eng.*, 2012, **29**, 173–181.

133 L. Wannatong, A. Sirivat and P. Supaphol, *Polym. Int.*, 2004, **53**, 1851–1859.

134 C. J. Luo, E. Stride and M. Edirisinghe, *Macromolecules*, 2012, **45**, 4669–4680.

135 S. Tungprapa, T. Puangparn, M. Weerasombut, I. Jangchud, P. Fakum, S. Semongkhol, C. Meechaisue and P. Supaphol, *Cellulose*, 2007, **14**, 563–575.

136 Z. J. Krysiak, Ł. Kaniuk, S. Metwally, P. K. Szewczyk, E. A. Sroczyk, P. Peer, P. Lisiecka-Graca, R. J. Bailey, E. Bilotti and U. Stachewicz, *ACS Appl. Bio Mater.*, 2020, **3**, 7666–7676.

137 V. Beachley and X. Wen, *Mater. Sci. Eng., C*, 2009, **29**, 663–668.

138 A. H. Hekmati, A. Rashidi, R. Ghazisaeidi and J. Y. Drean, *Text. Res. J.*, 2013, **83**, 1452–1466.

139 M. M. Jacobs Valencia and R. D. Anandjiwala, *J. Appl. Polym. Sci.*, 2010, **115**, 3130–3136.

140 G. Yazgan, R. I. Dmitriev, V. Tyagi, J. Jenkins, G. M. Rotaru, M. Rottmar, R. M. Rossi, C. Toncelli, D. B. Papkovsky, K. Maniura-Weber and G. Fortunato, *Sci. Rep.*, 2017, **7**, 1–13.

141 H. Fashandi and M. Karimi, *Polymer*, 2012, **53**, 5832–5849.

142 R. M. Nezarati, M. B. Eifert and E. Cosgriff-Hernandez, *Tissue Eng., Part C*, 2013, **19**, 810–819.

143 B. Zaarour, L. Zhu, C. Huang and X. Jin, *Nanoscale Res. Lett.*, 2018, **13**, 285.

144 C. L. Pai, M. C. Boyce and G. C. Rutledge, *Macromolecules*, 2009, **42**, 2102–2114.

145 K. Tanaka, M. Tomizawa and T. Katayama, *Mech. Eng. J.*, 2016, **3**, 16.

146 W. Liu, C. Huang and X. Jin, *Nanoscale Res. Lett.*, 2014, **9**, 350.

147 D. Zhang, P. Davoodi, X. Li, Y. Liu, W. Wang and Y. Y. S. Huang, *Sci. Rep.*, 2020, **10**, 1–9.

148 F. Sepúlveda, N. Butto, J. L. Arias, M. Yazdani-Pedram, P. K. Szewczyk, A. Gruszczynski, U. Stachewicz and A. Neira-Carrillo, *Cryst. Growth Des.*, 2020, **20**, 5610–5625.

149 S. Kim, H. Park and H. Choi, *Microporous Mesoporous Mater.*, 2019, **281**, 23–31.

150 T. Busolo, D. P. Ura, S. K. Kim, M. M. Marzec, A. Bernasik, U. Stachewicz and S. Kar-Narayan, *Nano Energy*, 2019, **57**, 500–506.

151 H. W. Tong and M. Wang, *Mater. Lett.*, 2013, **94**, 116–120.

152 H. W. Tong, M. Wang and W. W. Lu, *Nanomedicine*, 2013, **8**, 577–589.

153 D. P. Ura, J. Rosell-Llompart, A. Zaszczyńska, G. Vasilyev, A. Gradys, P. K. Szewczyk, J. Knapczyk-Korczak, R. Avrahami, A. O. Šišková, A. Arinstein, P. Sajkiewicz, E. Zussman and U. Stachewicz, *Materials*, 2020, **13**, 4169.

154 O. Urbanek, P. Sajkiewicz and F. Pierini, *Polymer*, 2017, **124**, 168–175.

155 H. W. Tong and M. Wang, *Biomed. Mater.*, 2010, **5**, 054110.

156 D. P. Ura, J. Knapczyk-Korczak, P. K. Szewczyk, E. A. Sroczyk, T. Busolo, M. M. Marzec, A. Bernasik, S. Kar-Narayan and U. Stachewicz, *ACS Nano*, 2021, **15**, 8848–8859.

157 S. Pawłowska, C. Rinoldi, P. Nakielski, Y. Ziai, O. Urbanek, X. Li, T. A. Kowalewski, B. Ding and F. Pierini, *Adv. Mater. Interfaces*, 2020, **7**, 1–13.

158 Y. Liu, X. Zhang, Y. Xia and H. Yang, *Adv. Mater.*, 2010, **22**, 2454–2457.

159 H. J. Nieminen, I. Laidmäe, A. Salmi, T. Rauhala, T. Paulin, J. Heinämäki and E. Hæggström, *Sci. Rep.*, 2018, **8**, 1–6.

160 B. Bhushan and Y. Chae Jung, *Ultramicroscopy*, 2007, **107**, 1033–1041.

161 J. Knapczyk-Korczak, P. K. Szewczyk and U. Stachewicz, *RSC Adv.*, 2021, **11**, 10866–10873.

162 M. S. Birajdar and J. Lee, *Macromol. Mater. Eng.*, 2015, **300**, 1108–1115.

163 M. A. K. Azad, T. Krause, L. Danter, A. Baars, K. Koch and W. Barthlott, *Langmuir*, 2017, **33**, 5555–5564.

164 B. White, A. Sarkar and A. M. Kietzig, *Appl. Surf. Sci.*, 2013, **284**, 826–836.

165 M. Liang, X. Chen, Y. Xu, L. Zhu, X. Jin and C. Huang, *Nanoscale*, 2017, **9**, 16214–16222.

166 D. Li, Y. Fan, G. Han and Z. Guo, *Chem. Eng. J.*, 2021, **404**, 126515.

167 S. J. Lee, N. Ha and H. Kim, *ACS Sustainable Chem. Eng.*, 2019, **7**, 10561–10569.

168 M. Cao and L. Jiang, *Surf. Innovations*, 2016, **4**, 180–194.

169 B. Bhushan, *Philos. Trans. R. Soc., A*, 2019, **377**, 20180274.

170 J. C. Cremaldi and B. Bhushan, *Beilstein J. Nanotechnol.*, 2018, **9**, 907–935.

171 B. Bhushan, *Philos. Trans. R. Soc., A*, 2009, **367**, 1445–1486.

172 H. Zhou, X. Jing and Z. Guo, *J. Colloid Interface Sci.*, 2020, **561**, 730–740.

173 H. Zhou, M. Zhang, C. Li, C. Gao and Y. Zheng, *Small*, 2018, **14**, 1–7.

174 G. Huang, H. Xu, Y. Jin, L. Huo, J. Zhao and Z. Li, *Mater. Lett.*, 2021, **289**, 129424.

175 J. Li, W. Li, X. Han and L. Wang, *J. Colloid Interface Sci.*, 2021, **581**, 545–551.

176 D. Wang, Y. Yue, Q. Wang, W. Cheng and G. Han, *Appl. Surf. Sci.*, 2020, **510**, 145462.

177 D. G. Yu, J. J. Li, M. Zhang and G. R. Williams, *Chem. Commun.*, 2017, **53**, 4542–4545.

178 A. Salama, A. Mohamed, N. M. Aboamera, T. Osman and A. Khattab, *Adv. Polym. Technol.*, 2018, **37**, 2446–2451.

179 N. Kurokawa, S. Kimura and A. Hotta, *J. Appl. Polym. Sci.*, 2018, **135**, 1–9.

180 M. Cai, H. He, X. Zhang, X. Yan, J. Li, F. Chen, D. Yuan and X. Ning, *Nanomaterials*, 2018, **9**, 39.

181 H. Zhou and Z. Guo, *J. Mater. Chem. A*, 2019, **7**, 12921–12950.

182 M. Cao, J. Xiao, C. Yu, K. Li and L. Jiang, *Small*, 2015, **11**, 4379–4384.

183 D. Chen, J. Li, J. Zhao, J. Guo, S. Zhang, T. A. Sherazi, Ambreen and S. Li, *J. Colloid Interface Sci.*, 2018, **530**, 274–281.

184 B. S. Lalia, S. Anand, K. K. Varanasi and R. Hashaikeh, *Langmuir*, 2013, **29**, 13081–13088.

185 J. Wu, H. Zhou, H. Wang, H. Shao, G. Yan and T. Lin, *Adv. Mater. Interfaces*, 2019, **6**, 1–9.

186 Z. Yu, H. Zhang, J. Huang, S. Li, S. Zhang, Y. Cheng, J. Mao, X. Dong, S. Gao, S. Wang, Z. Chen, Y. Jiang and Y. Lai, *J. Mater. Sci. Technol.*, 2021, **61**, 85–92.

187 P. Ke, X. N. Jiao, X. H. Ge, W. M. Xiao and B. Yu, *RSC Adv.*, 2014, **4**, 39704–39724.

188 Q. Liu, B. Wu, Z. Wang and T. Hao, *Atmosphere*, 2020, **11**, 258.

189 S. Montecinos, D. Carvajal, P. Cereceda and M. Concha, *Atmos. Res.*, 2018, **209**, 163–169.

190 D. V. Hung, S. Tong, Y. Nakano, F. Tanaka, D. Hamanaka and T. Uchino, *Biosyst. Eng.*, 2010, **107**, 54–60.

191 Y. Tian, P. Zhu, X. Tang, C. Zhou, J. Wang, T. Kong, M. Xu and L. Wang, *Nat. Commun.*, 2017, **8**, 1–8.

192 X. Tian, Y. Chen, Y. Zheng, H. Bai and L. Jiang, *Adv. Mater.*, 2011, **23**, 5486–5491.

193 H. Dong, N. Wang, L. Wang, H. Bai, J. Wu, Y. Zheng, Y. Zhao and L. Jiang, *ChemPhysChem*, 2012, **13**, 1153–1156.

194 Y. Liu, N. Yang, X. Li, J. Li, W. Pei, Y. Xu, Y. Hou and Y. Zheng, *Small*, 2020, **16**, 1–8.

195 C. Duprat, S. Protière, A. Y. Beebe and H. A. Stone, *Nature*, 2012, **482**, 510–513.

196 Z. Wang, A. Owais, C. Neto, J. M. Pereira and Y. Gan, *Adv. Mater. Interfaces*, 2021, **8**, 2–9.

197 R. Rutishauser, L. Wanntorp and E. Pfeifer, *Plant Syst. Evol.*, 2004, **248**, 219–241.

198 P. Zhu, R. Chen, C. Zhou, Y. Tian and L. Wang, *Chem. Eng. J.*, 2021, **415**, 128944.

199 J. Lin, X. Tan, T. Shi, Z. Tang and G. Liao, *ACS Appl. Mater. Interfaces*, 2018, **10**, 44815–44824.

200 S. Herminghaus, *Europhys. Lett.*, 2000, **52**, 165–170.

201 A. A. Babar, D. Miao, N. Ali, J. Zhao, X. Wang, J. Yu and B. Ding, *ACS Appl. Mater. Interfaces*, 2018, **10**, 22866–22875.

202 H. Liu and C. Tang, *Polym. J.*, 2007, **39**, 65–72.

203 H. Venkatesan, J. Chen, H. Liu, W. Liu and J. Hu, *Adv. Funct. Mater.*, 2020, **30**, 1–8.

204 Y. Chen, J. He, L. Wang, Y. Xue, Y. Zheng and L. Jiang, *J. Mater. Chem. A*, 2014, **2**, 1230–1234.

205 W. Chen and Z. Guo, *Nanoscale*, 2019, **11**, 15448–15463.

206 Y. Chen and Y. Zheng, *Nanoscale*, 2014, **6**, 7703–7714.

207 Y. Hou, Y. Chen, Y. Xue, Y. Zheng and L. Jiang, *Langmuir*, 2012, **28**, 4737–4743.

208 H. Bai, X. Tian, Y. Zheng, J. Ju, Y. Zhao and L. Jiang, *Adv. Mater.*, 2010, **22**, 5521–5525.

209 Y. Chen, D. Li, T. Wang and Y. Zheng, *Sci. Rep.*, 2016, **6**, 1–7.

210 H. Bai, R. Sun, J. Ju, X. Yao, Y. Zheng and L. Jiang, *Small*, 2011, **7**, 3429–3433.

211 Y. Chen, L. Wang, Y. Xue, Y. Zheng and L. Jiang, *Soft Matter*, 2012, **8**, 11450–11454.

212 Y. Y. Song, Y. Liu, H. B. Jiang, S. Y. Li, C. Kaya, T. Stegmaier, Z. W. Han and L. Q. Ren, *Sci. Rep.*, 2017, 7, 1–10.

213 P.-G. de Gennes, F. Brochard-Wyart and D. Quéré, in *Capillarity and Wetting Phenomena*, Springer New York, New York, 2004, pp. 1–32.

214 N. Thakur, A. S. Ranganath, K. Agarwal and A. Baji, *Macromol. Mater. Eng.*, 2017, 302, 1–9.

215 R. Hu, N. Wang, L. Hou, Z. Cui, J. Liu, D. Li, Q. Li, H. Zhang and Y. Zhao, *J. Mater. Chem. A*, 2019, 7, 124–132.

216 Q. Zhang, G. Lin and J. Yin, *Soft Matter*, 2018, 14, 8276–8283.

217 H. Dong, Y. Zheng, N. Wang, H. Bai, L. Wang, J. Wu, Y. Zhao and L. Jiang, *Adv. Mater. Interfaces*, 2016, 3, 3–7.

218 B. Bhushan, Y. C. Jung and K. Koch, *Philos. Trans. R. Soc., A*, 2009, 367, 1631–1672.

219 S. Al-Gharabli, B. Al-Omari, W. Kujawski and J. Kujawa, *Desalination*, 2020, 491, 114550.

220 S. Al-Gharabli, B. Al-Omari, W. Kujawski and J. Kujawa, *ACS Appl. Mater. Interfaces*, 2021, 13, 11268–11283.

221 R. N. Wenzel, *Ind. Eng. Chem.*, 1936, 28, 988–994.

222 A. B. D. Cassie, *Discuss. Faraday Soc.*, 1948, 3, 11–16.

223 G. McHale, *Langmuir*, 2007, 23, 8200–8205.

224 A. Marmur, *Langmuir*, 2003, 19, 8343–8348.

225 A. Tuteja, W. Choi, M. Ma, J. M. Mabry, S. A. Mazzella, G. C. Rutledge, G. H. McKinley and R. E. Cohen, *Science*, 2007, 318, 1618–1622.

226 H. Princen, *J. Colloid Interface Sci.*, 1970, 34, 171–184.

227 C. M. Regalado and A. Ritter, *Atmos. Res.*, 2016, 178–179, 45–54.

228 U. Stachewicz, F. Modaresifar, R. J. Bailey, T. Peijs and A. H. Barber, *ACS Appl. Mater. Interfaces*, 2012, 4, 2577–2582.

229 A. Almasian, G. Chizari Fard, M. Mirjalili and M. Parvinzadeh Gashti, *J. Ind. Eng. Chem.*, 2018, 62, 146–155.

230 M. N. Uddin, F. J. Desai, M. M. Rahman and R. Asmatulu, *Nanoscale Adv.*, 2020, 2, 4627–4638.

231 F. Bai, J. Wu, G. Gong and L. Guo, *Adv. Sci.*, 2015, 2, 1–6.

232 N. Shigezawa, F. Ito, Y. Murakami, S. Yamanaka and H. Morikawa, *J. Text. Inst.*, 2015, 107, 1014–1021.

233 J. Knapczyk-Korczak, P. K. Szewczyk, D. P. Ura, R. J. Bailey, E. Bilotti and U. Stachewicz, *Sustainable Mater. Technol.*, 2020, 25, e00191.

234 J. Knapczyk-Korczak, P. K. Szewczyk, D. P. Ura, K. Berent and U. Stachewicz, *RSC Adv.*, 2020, 10, 22335–22342.

235 V. A. Ganesh, A. S. Ranganath, A. Baji, H. K. Raut, R. Sahay and S. Ramakrishna, *Macromol. Mater. Eng.*, 2017, 302, 1600387.

236 P. K. Szewczyk, S. Metwally, J. E. Karbowniczek, M. M. Marzec, E. Stodolak-Zych, A. Gruszczyński, A. Bernasik and U. Stachewicz, *ACS Biomater. Sci. Eng.*, 2019, 5, 582–593.

237 X. Yan, M. Yu, S. Ramakrishna, S. J. Russell and Y. Z. Long, *Nanoscale*, 2019, 11, 19166–19178.